ISSN 1330-3651 (Print), ISSN 1848-6339 (Online) https://doi.org/10.17559/TV-20240823001936
Original scientific paper

Study on Air Duct Conversion and Extension Diagnosis of Booster Equipment in Audio Management Module of Airborne Electronic Equipment

Xiaomin XIE*, Xuanfu DU, Shuguo GUI

Abstract: In view of the failure situation that the air duct conversion structure in the audio management module cabin and the booster equipment conflict with each other in the functions of boosting ventilation and heat exchange ventilation, the air duct conversion mechanism arranged at the front end of the booster fan can realize the switching of external circulation, internal circulation and internal-external mixed circulation ventilation, and can adjust the ventilation volume of fresh air according to the actual working conditions. In this study, the ventilation booster adopts PWM speed regulation, and the power switch of the fan adopts self-developed intelligent power electronic switch, which can realize the overall power supply on-off control of the fan, and the speed of the fan is adjusted by PWM signal duty ratio, thus realizing the stepless speed regulation of 0~100% of the fan speed. The PWM speed control method fills the gap in this field and is more efficient than the traditional method to solve the conflict problem. One-stage power supply on-off control, two-stage speed adjustment control and two-stage control improve the reliability of the control circuit. The difficulty of integrating the two systems lies in the matching of air demand and fan performance in different working modes. Through the calculation of air duct resistance, booster ventilation and heat exchange ventilation in different working modes of air conditioning evaporation unit, reasonable fan performance parameters are obtained to guide the matching design of fans, thus eliminating the difficulty of conflict between booster ventilation and heat exchange ventilation.

Keywords: air duct conversion; supercharging equipment; PWM speed regulation

1 INTRODUCTION

In order to design four air supply modes of the environmental control system, the air duct converter consists of a wind direction distribution box, a motor, a slip ring, an outdoor fresh air interface, an indoor return air interface, a canister interface, an internal air duct air supply interface and a sealing structure, as shown in Figure 1. The motor of the air duct converter is controlled by comprehensive electronic control, and the sliding ring is driven to rotate by stepping rotation as required [1-5]. A method based on CFD simulation is proposed to optimize the design of air duct, and the best design scheme is found by simulating different geometric parameters, thus reducing the resistance loss of the system and improving the overall efficiency of the system [6-9]. The sliding ring is a semi-enclosed ring structure with a notch, where the air supply channel is located, and the rest of the air duct is closed by a sealing structure. Several energy-saving technologies, such as frequency conversion drive technology, cogeneration system and phase change energy storage technology, are also introduced, and the energy-saving effects of these technologies in practical application are proved by case studies [10-13]. Flexible graphite is selected as the sealing material, which not only ensures the sealing performance, but also reduces the friction when the slip ring rotates because of its self-lubricating ability [14-19]. The use status of the four air supply modes of the environmental control system is as follows:

(1) External circulation poison filtration mode: In this mode, the return air and the internal air duct in the cabin are closed, and the interface between the fresh air outlet outside the cabin and the poison canister is opened. At this time, the fresh air outside the cabin enters the air duct converter after dust removal and is supplied to the poison canister;

(2) External circulation non-poison filtration mode: In this mode, the air return port in the cabin and the interface of the poison filtration tank are closed, and the fresh air outlet outside the cabin and the internal air duct are opened. At this time, the fresh air outside the cabin enters the air duct converter after dust removal and is supplied to the internal air duct;

(3) Mixed circulation mode: in this mode, the interface of the canister is closed, and the fresh air outlet outside the cabin, the return air in the cabin and the inner air duct are opened. Among them, due to the large flow resistance of outdoor fresh air passing through cyclone dust collector, it is necessary to block some indoor air return openings, and the proportion of fresh air in mixed air can be continuously adjusted from 0 to 100%;

(4) Internal circulation mode: In this mode, the interface of the canister and the fresh air outlet outside the cabin are closed, and the air return outlet inside the cabin and the internal air duct are opened. At this time, the return air inside the cabin enters the air duct converter and is supplied to the internal air duct.

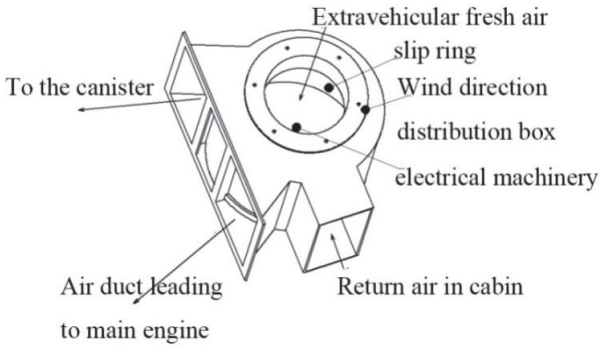

Figure 1 Schematic diagram of air duct converter structure

Air duct converter of airborne electronic equipment can optimize energy efficiency. By automatically controlling the operation mode of the air conditioning system, the operation mode of the air conditioning system is automatically switched according to the current climate conditions, so as to improve energy efficiency and reduce energy consumption. For example, when the outdoor

temperature is high, the converter will automatically switch to the cooling mode to reduce the indoor temperature and maintain a comfortable environment. When the outdoor temperature is low, it will switch to the heating mode to heat the indoor air and keep it warm. The air duct converter of airborne electronic equipment also improves the safety and energy saving effect.

The air duct converter of airborne electronic equipment also improves the safety and energy saving effect. By automatically controlling the operation mode of air conditioning system, the safety risk caused by improper human operation can be avoided. At the same time, energy consumption can be reduced by optimizing the operation efficiency of air conditioning system.

2 PERFORMANCE CALCULATION AND ANALYSIS OF CYCLONE DUST COLLECTOR

High efficiency axial cyclone dust collector is used to separate dust in the air. Dust-laden air enters the dust collector axially, and under the action of the deflector, the airflow turns into spiral motion, and the dust particles are in the centrifugal force field and thrown to the inner surface of the cylinder by centrifugal force. Under the scouring of the rotating airflow, the dust is discharged from the gap between the cylinder and the tail. The structural dimensions of the cyclone in this system are shown in Fig. 2.

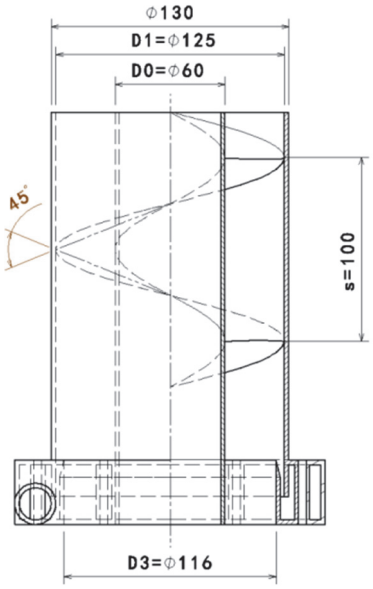

Figure 2 Structure diagram of cyclone dust collector

2.1 Calculation of dust removal performance

The force analysis of dust particles in the dust collector shows that the dust particles enter the dust collector with air, and the initial velocity υ_0 is in the same direction as the air flow. During the dust removal process, the dust particles mainly move along the radial direction, and the vertical movement component is ignored [20]. The particles are mainly affected by centrifugal force F_ω, air resistance F_R, viscous resistance F_μ and gravity G. According to Bernoulli equation $P+\frac{1}{2}\rho V^2+\rho gh=C$. The force analysis diagram of dust particles is shown in Fig. 3.

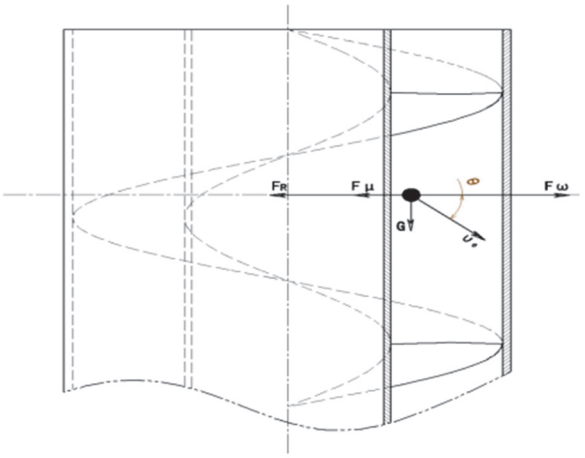

Figure 3 Force analysis diagram of dust particles

The vertical component of the initial velocity of dust particles υ_0 has no effect on the horizontal motion, and its horizontal component is $\upsilon_x = \upsilon_0 \times \cos\theta$. The velocity of dust particles is around 20 m/s, and the centrifugal acceleration is more than 7000 m/s^2, which is more than 700 times of the gravity acceleration of 9.8 m/s^2, so the gravity effect is ignored in this process. The dust particles are treated as spheres, and the windward surface is a hemisphere, on which all the air resistance and viscous resistance occur. The air resistance coefficient and viscous resistance coefficient are related to the shape and roughness of the windward surface. Here, the air resistance coefficient C = 1 is selected according to the extreme bad situation, that is, the windward air is stagnated and the dynamic pressure head of the air is completely consumed, and the viscous resistance is zero at this time.

According to the above principle, the force model of particles is simplified, and the particles have a horizontal initial velocity υ_x, and move from the center to the inner wall edge of the cylinder in the horizontal direction under the action of the resultant force F of centrifugal force F_ω and air resistance F_R, as shown in Fig. 4.

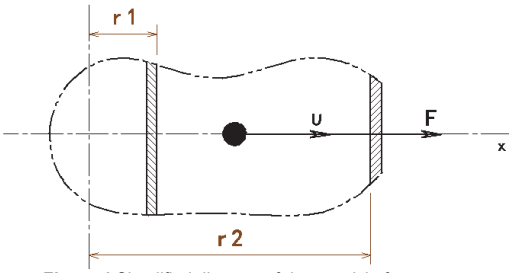

Figure 4 Simplified diagram of dust particle force

As shown in the structural diagram of the cyclone dust collector, when the swirl angle θ = 45, the length of the swirl part channel L = 464mm, the cross-sectional area of the swirl part channel $A_2 = a \times b$ = 3250 mm^2, and the air flow through the dust collector q_v = 300 m^3/h:

The velocity of air $\upsilon_0 = q_v/A_2$ = 25.64m/s.

Horizontal component velocity υ_x = 18.14m/s

Centrifugal force $F_\omega = m \times \alpha_\omega = 4\pi\rho(d/2)^3\upsilon^2/3(r_1 + dx)$ on particles.

The air resistance of particles $F_r = CS\rho_0\upsilon^2/2$.

where: m - dust particle mass, kg; P - dust particle density, 2300 kg/m^3; d - diameter of dust particle sphere, mm; υ - instantaneous velocity of dust particles, m/s;

r_1 - radius of cyclone dust collector guide core, $r_1 = 30$ mm; C - coefficient of particle air resistance, taking 1.0; S - windward area of particle sphere, mm^2, $S = \pi \times d^2/4$; ρ_0 - air density, taking 1.2 kg/m^3.

The cyclone angle $\theta = 30$ or 60, and the calculation and analysis of the cyclone channel length and the cyclone channel cross-sectional area are the same as $\theta = 45$, only the data can be changed, so I will not repeat them here.

The resultant force $F = F_\omega + F_R$, and the acceleration $\alpha = F/m$.

Taking the particle sphere as an infinitesimal element, the particle accelerates from the initial velocity v_1 to $v_1 + dv$, and the position moves from x_1 to $x_1 + dx$ after dt time. Because the dt time is very short, it can be considered that $[v_1 + (v_1 + dv)]/2$ is the average velocity during this time, then

$dx = dv^2/2\alpha + v_1 dv/\alpha$

When $x_1 = r_1$, $v_1 = v_x$, integrate dx from r_1 to r_2 and substitute it into the force analysis formula:

Diameter of dust particle sphere $d = 0.019$ mm = 19 μm;

The time required for dust particles to move from r_1 to r_2 is Δt =2.6 ms;

It takes $\Delta t = L/v_0 = 18.1$ ms for air to move from cyclone inlet to cyclone outlet, which is much longer than the time δt for dust particles to hit the wall, so dust particles can be filtered out.

To sum up, the cyclone dust collector can theoretically filter out 100% dust particles with a diameter of more than 19 μm. When the air volume is 100 m^3/h, the cyclone can also filter out 100% of dust particles above 19 μm, only the time for dust particles to hit the wall is increased from 2.6 ms to 7.7 ms.

2.2 Calculation and Analysis of Flow Resistance

According to the structure diagram of cyclone, the structural parameters of cyclone are as follows:

Swirl angle $\theta = 45°$.

Cyclone inlet ring area $A_1 = \pi \times (D_1^2 - D_0^2)/4 = 9440$ mm^2.

Cross-sectional area of the cyclone channel $A_2 = s \times (D_1 - D_0)/2 = 3250$ mm^2.

The area of cyclone outlet ring $A_3 = \pi \times (D_3^2 - D_0^2)/4 = 7737$ mm^2.

The length of the cyclone part flow channel $L = 464$ mm.

Hydraulic diameter of cyclone part $d = (D_1 - D_0) \times s/[(D_1 - D_0)/2 + s] = 49$ mm.

Air density $\rho = 1.2$ kg/m^3.

Aerodynamic viscosity $\mu = 0.025 \times 10^{-3}$ Pa·s.

Air kinematic viscosity $v = \mu/\rho = 20.83 \times 10^{-6}$ m^2/s

When the air flow through the dust collector $q_v = 300$ m^3/h:

Air velocity $v = q_v/A_2 = 25.64$ m/s.

Reynolds number $Re = v \times d/v = 60377 > 2300$, and the flow is turbulent.

Roughness of cylinder and guide vane wall $\varepsilon = 0.01$ mm.

Relative roughness $\varepsilon/d = 0.0002$.

The thickness of viscous bottom layer $\delta = 34.2d/Re^{0.875} = 0.11$ mm.

$\delta/\varepsilon = 11 > 1$, which can be regarded as hydraulic smoothness, so the flow is in the turbulent smooth tube area (1.75th power resistance area).

Because $Re < 10^5$:

Along the way loss coefficient $\lambda = 0.3164Re^{0.25} = 0.0202$.

Along the way loss $h_f = \lambda L v^2/(2gd) = 64$ m air column.

The air enters the swirl channel A_2 from the circular section $A1$ of the inlet, which is a process of decreasing section. The local loss coefficient $\zeta_1 = \lambda\ [1 - (A_2/A_1)^2]/\sin(\theta/2) = 0.0465$. The air moves around the circle for 1.5 times in the swirl channel, which is equivalent to passing through six 90 bends continuously. The local loss coefficient $\zeta_2 = 6 \times [0.131 + 0.163(d/R)^{3.5}] = 1.988$.

Air enters the outlet circular section $A3$ from the swirl channel A_2, which is a process of gradually expanding the section, and the local loss coefficient $\zeta_3 = (1 - A_2/A_3)^2 = 0.3363$.

Total local loss coefficient $\zeta = \Sigma\zeta_i = 2.3708$.

Local loss $h_j = \zeta \times v^2/2g = 79.53$ m air column.

Flow resistance $\Delta P = h_f + h_j = 85.93$ m air column = 1011 Pa.

Compared with a mature product of the same type, this type of cyclone dust collector is shown in Tab. 1.

Table 1 Comparison of two axial-flow cyclone dust collectors

Serial number	Parameter	This type of product	Mature product
1	Handling air volume	300 m^3/h	33.8 m^3/h
2	Diameter of diversion core	60 mm	25 mm
3	Cylinder radius	130 mm	50 mm
4	Cylinder height	210 mm	120 mm
5	Lead	100 mm	35 mm
6	Swirl angle	45°	25°
7	Swirl number	1.5 laps	2 laps
8	Minimum 100% dust particle diameter	19 μm	12 μm
9	Flow resistance	1011 Pa	470 Pa

Through analysis, it can be seen that this product can handle much larger air volume than the original product in a limited installation space with little difference in performance, which is suitable for this scheme.

3 DESIGN AND ANALYSIS OF AIR DUCT CONVERSION AND CLOSING MECHANISM OF BOOSTER EQUIPMENT

In order to prevent the tropospheric shock wave from impacting the interior of the cabin, the automatic quick closing technology must be adopted for the external hatch cover of the system communicating with the cabin, and the quick closing time index is no more than 0.15 s.

There are three external covers of the environmental control system, among which the extravehicular environmental detection module is not connected with the cabin, and the other two are the fresh air inlet and exhaust outlet in the cabin, which need to be designed with quick closing machines [21-24]. The design principle of the new air outlet closing machine is the same as that of the air outlet closing machine. The quick electric push-pull rod drives the movable door to open and close, and the driving force is 50 N. The quick push-pull rod is a fast-shrinking and slow-stretching type, the retraction rate is 230 mm/s,

the closing stroke of the mechanism is designed to be 30mm, and the retraction time is 0.13 s, which meets the requirements of quick closing. Use high-quality sealing materials (such as silica gel, EPDM rubber, etc.) at the joint of the pipeline to ensure the tightness of the joint. On the premise of ensuring sufficient strength, choosing lighter materials can reduce the installation cost and structural burden. Using CFD (computational fluid dynamics) and other tools to simulate the pipeline system, optimize the design parameters, and ensure the best performance in practical application. Consider the integration of the whole HVAC system, and ensure the coordination of various components, such as fans and pipes, cooling towers and heat exchangers, to work together to improve the overall energy efficiency.

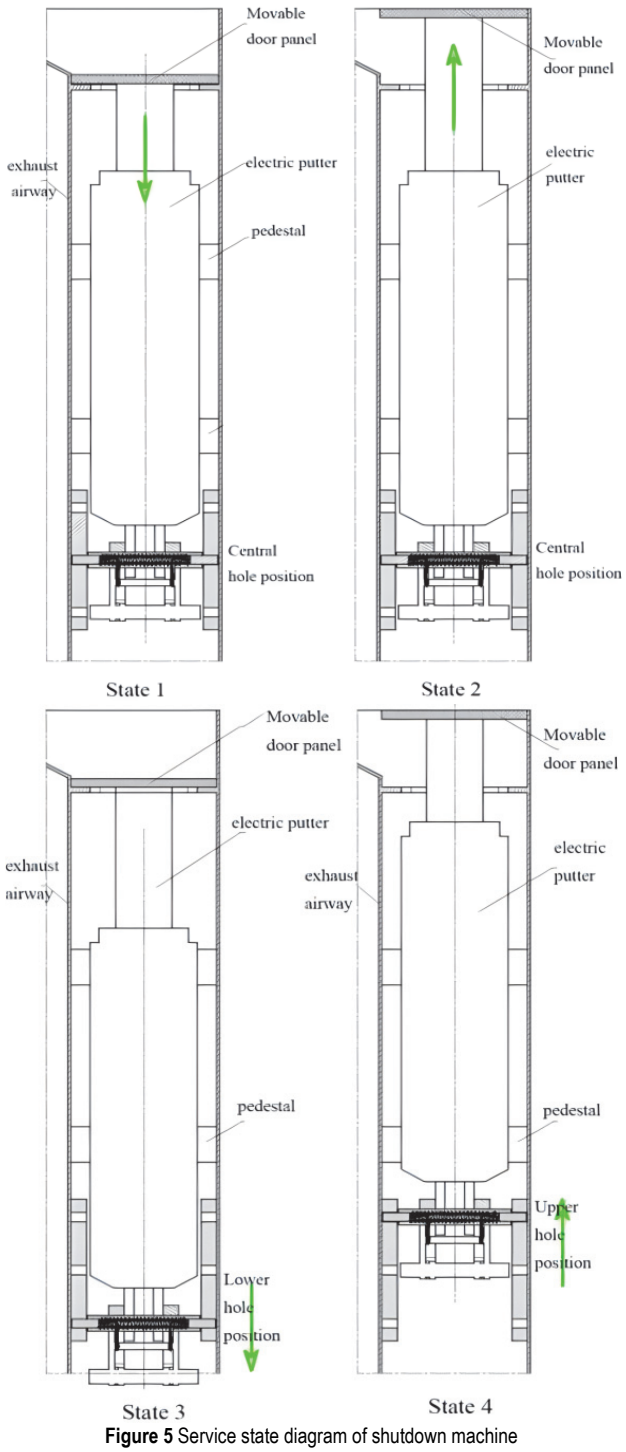

Figure 5 Service state diagram of shutdown machine

The smaller the elbow angle in the pipeline, the greater the energy loss when the fluid turns. Therefore, choosing a larger elbow radius is helpful to reduce energy loss. Using efficient thermal insulation materials (such as polyurethane foam, phenolic foam, etc.) can significantly reduce the heat exchange caused by the temperature difference between inside and outside the pipeline. When the movable door panel needs to be moved, the cable sliding rod is pulled manually, and the movable pin is pulled back into the sleeve through the cable to release the limit state, so that the electric push-pull rod and the movable door panel can move integrally by pushing and pulling the hand lever [25]. When the movable pin moves to the upper hole position or the lower hole position, the cable sliding rod is released, and the movable pin pops out of the sleeve under the action of the spring in the sleeve to form the limit again.The use state diagram of the shutdown machine is shown in Fig. 5.

There are four use states of the shutdown machine:

(1) Automatic closing: the movable pin is limited at the central hole, the arm of the electric push-pull rod retracts for 30 mm after receiving the comprehensive control instruction for 0.13 s, and the movable door plate is attached to the sealing surface to form rapid automatic closing;

(2) Automatic opening: the movable pin is limited at the central hole, the arm of the electric push-pull rod extends out after receiving the comprehensive control instruction, and the movable door plate is separated from the sealing surface to form automatic opening;

(3) Manual closing: when the arm of the electric push-pull rod is stuck in the open state and the movable door panel needs to be closed at this time, the limit of the movable pin can be released, and when the handle is pulled back to the lower hole position, the movable door panel is attached to the sealing surface to limit the movable pin again after manual closing;

(4) Manual opening: when the arm of the electric push-pull rod is stuck in the closed state and the movable door panel needs to be opened at this time, the limit of the movable pin can be released, and when the handle is pushed out to the upper hole position, the movable door panel is separated from the sealing surface, so that the movable pin can be limited again after manual opening.

Automatic closing force check:

(1) The closing direction of the fresh air inlet closing machine is in the same direction as the airflow, and there is no airflow resistance, that is, there is no closing resistance;

(2) The closing direction of the exhaust ventilator is opposite to the airflow, and it will be resisted by airflow when it is closed. The flow area of the exhaust duct is a = 117 × 75 mm. When the air supply of the system is at the maximum air volume of 500 m^3/h, wind speed $v = q_v/A$ = 15.8 m/s, dynamic head $P = \rho v^2/2$ = 150 Pa.

The resistance $F = P \times A$ = 1.3 N, which is far less than the closing force 50 N of the electric push-pull rod. Assuming that the dynamic head reaches 500 Pa, the resistance $F = P \times A$ = 4.3 N, which is far less than the closing force 50 N of the electric push-pull rod.

When the system detects the high radiation alarm signal, quickly close the air inlet and the exhaust and dust removal port to prevent the shock wave from damaging the inside of the unit, and enter the pressurization and poison

filtration protection after a delay of 50 seconds [26]. When low radiation alarm or poison alarm is detected, it will directly enter the pressurization poison filter protection. First, quickly switch the air duct to the poison filtration mode. Turn on the air intake valve, close the exhaust control valve, start the booster fan, activate the dust outlet valve, and engage the pressurized poison filtration function. Next, adjust the fan speed and the position of the exhaust valve based on the real-time detected cabin overpressure and the amount of fresh air. Ensure that the cabin overpressure remains at least 300 Pa and that the fresh air volume meets the passengers' needs during the defense mode. If no three-defense alarm signal is detected, switch the air duct back to the normal ventilation mode. The control flow of the three-prevention function is shown in Fig. 6.

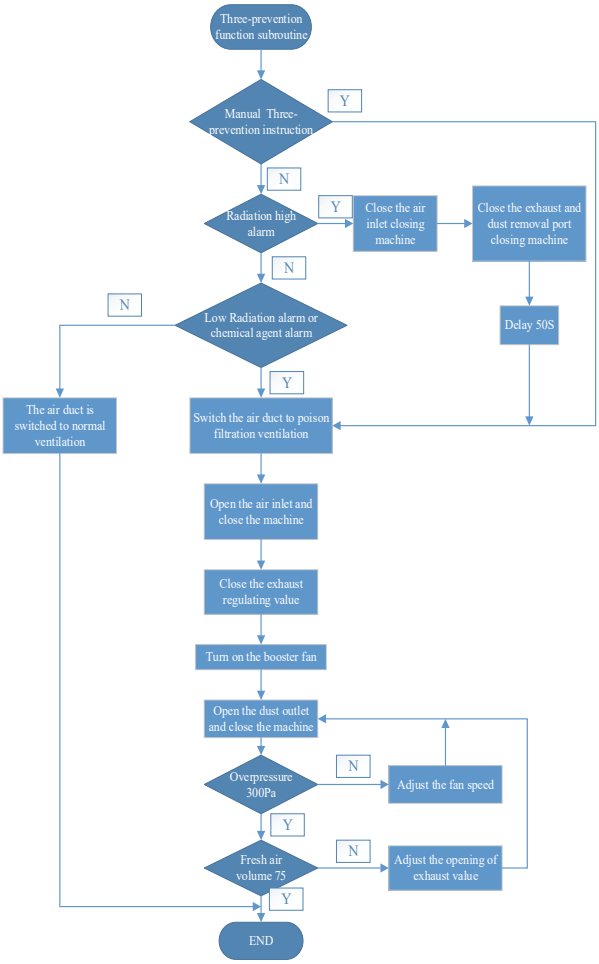

Figure 6 Three-prevention function control flow chart

When controlling the ventilation function, if the system is in three-proof mode, it prioritizes ensuring the pressurization needed for three-proof protection. The system follows the three-proof control logic to manage ventilation. In the non-three-proof mode, the system gives priority to the exhaust demand after fire fighting and explosion suppression in the cabin [27, 28]. If there is fire fighting action, the air inlet shutoff machine and exhaust shutoff machine are quickly turned on, and the booster fan is turned on for external air circulation. In the ordinary ventilation function, according to the different ventilation modes, the mechanisms such as air inlet closers, air exhaust and dust outlet closers, air exhaust regulating valves and air return openings are controlled to make the system run in different ventilation modes, and then the booster fan is turned on to realize the ventilation function. In the ventilation modes of external circulation and mixed internal and external circulation, the system adjusts the fan speed and the opening of the exhaust control valve according to the cabin overpressure and fresh air volume, ensuring that the cabin overpressure is not less than 100 Pa and the fresh air volume meets the needs of passengers. In general driving operation, the fresh air volume is not less than 34 m^3/h/person, and in fire fighting operation, the fresh air volume is not less than 100 m^3/h/person.

4 STUDY ON CALCULATION AND ANALYSIS OF AIR DUCT CONVERSION RESISTANCE

There are four ventilation states in this system, namely, external circulation filtering state, external circulation non-filtering state, mixed circulation state and internal circulation state. The resistance components of the system include cyclone dust collector, air duct in the main engine, canister, evaporator core and cabin passenger air duct.

4.1 Calculation and Analysis of Mixed Circulation State and Internal Circulation State

In the mixed circulation state, 500 m^3/h of mixed air is required, including 100 m^3/h of fresh air and 400 m^3/h of internal circulation air. The resistance components include cyclone dust collector, main engine internal air duct, evaporator core and cabin passenger air duct.

(1) Calculation of cyclone resistance

According to the structure diagram of cyclone dust collector, the parameters are as follows:

Swirl angle $\theta = 45$.

Cyclone inlet ring area $A_1 = \pi \times (D_1^2 - D_0^2)/4 = 9440$ mm^2.

Cross-sectional area of the cyclone channel $A_2 = s \times (D_1 - D_0)/2 = 3250$ mm^2.

The area of cyclone outlet ring $A_3 = \pi \times (D_3^2 - D_0^2)/4 = 7737$ mm^2.

The length of the cyclone part flow channel $L = 464$ mm.

Hydraulic diameter of cyclone part $d = (D_1 - D_0) \times s/[(D_1 - D_0)/2 + s] = 49$ mm.

Air density $\rho = 1.2$ kg/m^3.

Aerodynamic viscosity $\mu = 0.025 \times 10^{-3}$ Pa·s.

Air kinematic viscosity $v = \mu/\rho = 20.83 \times 10^{-6}$ m^2/s.

When the air flow through the dust collector $q_v = 100$ m^3/h:

Air velocity $v = q_v / A_2 = 8.55$ m/s.

Reynolds number $Re = v \times d/v = 20126 > 2300$, and the flow is turbulent.

Roughness of cylinder and guide vane wall $\varepsilon = 0.01$ mm.

Relative roughness $\varepsilon/d = 0.0002$.

The thickness of viscous bottom layer $\delta = 34.2d/Re^{0.875} = 0.288$ mm.

$\delta/\varepsilon = 28.77 > 1$, which can be regarded as hydraulic smoothness, so the flow is in the turbulent smooth tube area (1.75th power resistance area).

Because $Re < 10^5$:

Along the way loss coefficient $\lambda = 0.3164/Re^{0.25} = 0.0266$.

Along the way loss $h_f = \lambda Lv^2/(2gd) = 0.94$ air column.

The air enters the swirl channel A_2 from the circular section A_1 of the inlet, which is a process of decreasing section. The local loss coefficient $\zeta_1 = \lambda[1 - (A_2/A_1)^2]/\sin(\theta/2) = 0.0612$.

The air moves around the circle for 1.5 times in the swirl channel, which is equivalent to passing through six 90 bends continuously. The local loss coefficient $\zeta_2 = 6 \times [0.131 + 0.163(d/R)^{3.5}] = 1.988$.

Air enters the outlet circular section A_3 from the swirl channel A_2, which is a process of gradually expanding the section, and the local loss coefficient $\zeta_3 = (1 - A_2/A_3)^2 = 0.3363$.

Total local loss coefficient $\zeta = \Sigma\zeta_i = 2.3855$.

Local loss $h_j = \zeta \times v^2/2g = 8.89$ air column.

Flow resistance $\Delta P = h_f + hj = 9.83$ air column =116 Pa.

(2) Calculation of evaporator core resistance

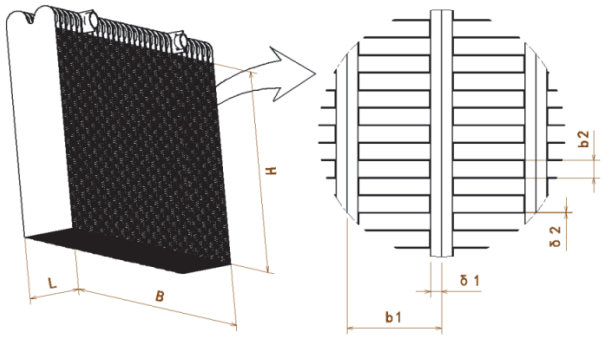

Figure 7 Structure diagram of evaporator core

The structure diagram of evaporator core is shown in Fig. 7, and the parameters are as follows: height $H = 215$ mm; width $B = 300$ mm; thickness $L = 58$ mm; upwind area $A_1 = H \times B = 64500$ mm^2; partition spacing b_1=10.8 mm; diaphragm thickness $\delta_1 = 1.5$ mm; fin spacing $b_2 = 2$ mm; fin thickness $\delta_2 = 0.1$ mm; ventilation area of fin unit $A_c = (b_1 - 2\delta_1 - \delta_2) \times (b_2 - \delta_2) = 15$ mm^2; number of fin units $n = (H/b_2) \times (B/b_1) = 2986$.

During the refrigeration process, liquid water droplets will precipitate in the evaporator fin channel, which will affect the ventilation area. Generally, the blocking rate is 0.25, and the total wet ventilation area $A_2 = 0.75 \times n \times A_c = 32765$ mm^2.

Wet circumference $U = 2 \times n \times (b_1 + b_2 - 2 \times \delta_1 - 2 \times \delta_2) = 57333$ mm.

Hydraulic diameter $d = 4 \times A_2/U = 2.29$ mm.

Air density $\rho = 1.2$ kg/m^3.

Aerodynamic viscosity $\mu = 0.025 \times 10^{-3}$ Pa·s.

Air kinematic viscosity $v = \mu/\rho = 20.83 \times 10^{-6}$ m^2/s.

When the air flow through the evaporator $q_v = 500$ m^3/h:

Air velocity $v = q_v/A_2 = 4.24$ m/s.

Reynolds number $Re = v \times d/v = 465$. Because the air has been in a turbulent state before entering the evaporator, the evaporator flow channel is short and the fins are provided with shutters, the air flow in the evaporator flow channel is still in a turbulent state.

Because the louvers are arranged on the fins, the roughness $\varepsilon = 0.5$ mm.

Relative roughness $\varepsilon/d = 0.2187$.

The thickness of viscous bottom layer $\delta = 34.2d/Re^{0.875} = 0.362$ mm.

$\delta/\varepsilon = 0.72 < 1$, which can be regarded as hydraulic roughness, so the flow is in the turbulent rough tube area.

The loss coefficient $\lambda = [2lg(d/2\varepsilon + 1.74)]^{-2} = 0.6833$.

Along the way loss $h_f = \lambda Lv^2/(2gd) = 15.89$ m air column.

Air enters the ventilation section A_2 of the core fin from the windward section A_1 of the inlet, which is a process of sudden contraction of the section, $A_2/A_1 = 0.508$, and the local loss coefficient $\zeta_1 = 0.298$.

The air returns to the outlet section A_1 through the ventilation section A_2 of the core, which is a sudden expansion process of the section, and the local loss coefficient $\zeta_2 = (1 - A_2/A_1)^2 = 0.2421$.

Total local loss coefficient $\zeta = \Sigma\zeta_i = 0.5401$.

Local loss $h_j = \zeta \times v^2/2g = 0.5$m air column.

Flow resistance $\Delta P = h_f + h_j = 16.39$ m air column = 193 Pa.

(3) Calculation of air duct resistance of cabin occupants

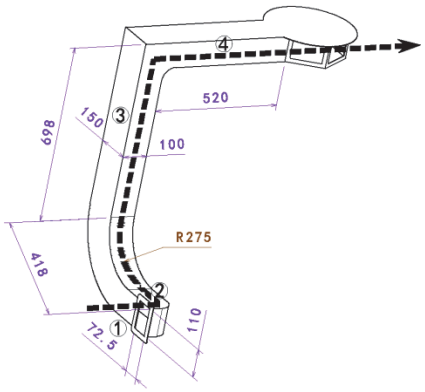

Figure 8 Schematic diagram of air duct resistance calculation

The structural diagram of cabin occupant air duct resistance is shown in Fig. 8, and the parameters are as follows:

Section 1 area $A_1 = 110 \times 72.5 = 7975$ mm^2.

Section 2 area $A_2 = 100 \times 72.5 = 7250$ mm^2.

Section 3 area $A_3 = 150 \times 100 = 15000$ mm^2.

Section 4 area $A_4 = 150 \times 100 = 15000$ mm^2.

Air duct length $L = 1636$ mm.

Average hydraulic diameter $d = 120$ mm.

Air density $\rho = 1.2$ kg/m^3.

Aerodynamic viscosity $\mu = 0.025 \times 10^{-3}$ Pa·s.

Air kinematic viscosity $v = \mu/\rho = 20.83 \times 10^{-6}$ m^2/s.

When the air flow through the air duct $q_v = 500$ m^3/h:

Air velocity $v = q_v/A_2 = 9.26$ m/s.

Reynolds number $Re = v \times d/v = 53333 > 4000$, and the flow is turbulent.

Roughness of cylinder and guide vane wall $\varepsilon = 0.01$ mm.

Relative roughness $\varepsilon/d = 0.0001$.

The thickness of viscous bottom layer $\delta = 34.2d/Re^{0.875} = 0.3$ mm.

$\delta/\varepsilon = 30 > 1$, which can be regarded as hydraulic smoothness, so the flow is in the turbulent smooth tube area (1.75th power resistance area).

Because $Re < 10^5$:

Along the way loss coefficient $\lambda = 0.3164/Re^{0.25} = 0.0208$.

Along the way loss $h_f = \lambda Lv^2/(2gd) = 1.24$ m air column.

The air enters the section A_2 from the section A_1, and after right-angle turning, the local loss coefficient $\zeta_1 = 0.985$.

Air enters section A_3 from section A_2 and passes through a 90 elbow, resulting in local loss coefficient.

$\zeta_2 = 0.131 + 0.163(d/R)^{3.5} = 0.1399$.

Air suddenly expands from section A_2 to section A_3, and the local loss coefficient $\zeta_3 = (1 - A_2/A_3)^2 = 0.2669$.

Air enters the section A_4 from the section A_3, and after right-angle turning, the local loss coefficient $\zeta_1 = 0.985$.

Total local loss coefficient $\zeta = \Sigma\zeta_i = 2.3769$.

Local loss $h_j = \zeta \times v^2/2g = 10.40$ m air column.

Flow resistance $\Delta P = h_f + h_j = 11.64$ m air column = 137 Pa.

In the mixed circulation state, the mixed air is 500 m^3/h, and the total flow resistance is 571 Pa.

Compared with the mixed circulation state, the internal circulation state has fewer cyclone components, so the total flow resistance is less than 571 Pa at the same air volume of 500 m^3/h, which is included in the mixed circulation state.

4.2 Calculation and Analysis of External Circulation Ventilation State

Fresh air of 300 m^3/h is required in the non-poison-filtering state of external circulation, and the resistance components include cyclone dust collector, internal air duct of main engine, evaporator core and cabin passenger air duct.

(1) Calculation of air duct resistance in main engine

The structural parameters of the air duct in the main engine are the same as the maximum refrigeration state;

The air physical parameters are also the same;

When the air flow through the inner air duct $q_v = 300$ m^3/h:

Air velocity $v = q_v /A_2 = 4.73$ m/s.

Reynolds number $Re = v \times d/\nu = 27778 > 4000$, and the flow is turbulent.

Roughness of cylinder and guide vane wall $\varepsilon = 0.01$ mm.

Relative roughness $\varepsilon/d = 0.0001$.

The thickness of viscous bottom layer $\delta = 34.2d/Re^{0.875} = 0.541$ mm.

$\delta/\varepsilon = 54.1 > 1$, which can be regarded as hydraulic smoothness, so the flow is in the turbulent smooth tube area (1.75th power resistance area).

Because $Re < 10^5$:

Along the way loss coefficient $\lambda = 0.3164/Re^{0.25} = 0.0245$.

Along the way loss $h_f = \lambda Lv^2/(2gd) = 0.14$ m air column.

The air enters the section A_2 from the section A_1, and after right-angle turning, the local loss coefficient $\zeta_1 = 0.985$.

Air enters the section A_2 from the section A_1, and there is also the sudden expansion process of the section, and the local loss coefficient.

$\zeta_2 = (1 - A_1/A_2)^2 = 1.0$.

Air suddenly expands from section A_2 to section A_3, and the local loss coefficient $\zeta_3 = (1 - A_2/A_3)^2 = 0.5974$.

The air enters the section A_4 from the section A_3, and the local loss coefficient $\zeta_4 = 0.659$.

Total local loss coefficient $\zeta = \Sigma\zeta_i = 3.2414$.

Local loss $h_j = \zeta \times v^2/2g = 3.71$ m air column.

Flow resistance $\Delta P = h_f + h_j = 3.84$ m air column = 45 Pa.

(2) Calculation of evaporator core resistance

The structural parameters of evaporator core are the same as the maximum refrigeration state;

The air physical parameters are also the same;

When the air flow through the evaporator $q_v = 300$ m^3/h:

Air velocity $v = q_v /A_2 = 2.52$ m/s.

Reynolds number $Re = v \times d/\nu = 279$. Because the air has been in a turbulent state before entering the evaporator, the evaporator flow channel is short and the fins are provided with shutters, the air flow in the evaporator flow channel is still in a turbulent state.

Because the louvers are arranged on the fins, the roughness $\varepsilon = 0.5$ mm.

Relative roughness $\varepsilon/d = 0.2187$.

The thickness of viscous bottom layer $\delta = 34.2d/Re^{0.875} = 0.656$ mm.

$\delta/\varepsilon = 0.76 < 1$, which can be regarded as hydraulic roughness, so the flow is in the turbulent rough tube area.

The loss coefficient $\lambda = [2lg(d/2\varepsilon + 1.74)]^{-2} = 0.6833$.

Along the way loss $h_f = \lambda Lv^2/(2gd) = 5.72$ m air column.

Air enters the ventilation section A_2 of the core fin from the windward section A_1 of the inlet, which is a process of sudden contraction of the section, $A_2/A_1 = 0.508$, and the local loss coefficient $\zeta_1 = 0.298$.

The air returns to the outlet section A_1 through the ventilation section A_2 of the core, which is a sudden expansion process of the section, and the local loss coefficient $\zeta_2 = (1 - A_2/A_1)^2 = 0.2421$.

Total local loss coefficient $\zeta = \Sigma\zeta_i = 0.5401$.

Local loss $h_j = \zeta \times v^2/2g = 0.18$ m air column.

Flow resistance $\Delta P = h_f + h_j = 5.9$ m air column = 69 Pa.

(3) Calculation of air duct resistance of cabin occupants

The structural parameters of the cabin occupant air duct are the same as the maximum refrigeration state;

The air physical parameters are also the same;

When the air flow through the air duct $q_v = 300$ m^3/h:

Air velocity $v = q_v /A_2 = 5.56$ m/s.

Reynolds number $Re = v \times d/\nu = 32000 > 4000$, and the flow is turbulent.

Roughness of cylinder and guide vane wall $\varepsilon = 0.01$ mm.

Relative roughness $\varepsilon/d = 0.0001$.

The thickness of viscous bottom layer $\delta = 34.2d/Re^{0.875} = 0.469$ mm.

$\delta/\varepsilon = 46.9 > 1$, which can be regarded as hydraulic smoothness, so the flow is in the turbulent smooth tube area (1.75th power resistance area).

Because $Re < 10^5$:

Along the way loss coefficient $\lambda = 0.3164/Re^{0.25} = 0.0237$.

Along the way loss $h_f = \lambda Lv^2/(2gd) = 0.51$ m air column.

The air enters the section A_2 from the section A_1, and after right-angle turning, the local loss coefficient $\zeta_1 = 0.985$.

Air enters section A_3 from section A_2 and passes through a 90 elbow, resulting in local loss coefficient.

$\zeta_2 = 0.131 + 0.163(d/R)^{3.5} = 0.1399$.

Air suddenly expands from section A_2 to section A_3, and the local loss coefficient $\zeta_3 = (1 - A_2/A_3)^2 = 0.2669$.

Air enters the section A_4 from the section A_3, and after right-angle turning, the local loss coefficient $\zeta_1 = 0.985$.

Total local loss coefficient $\zeta = \Sigma\zeta_i = 2.3769$.

Local loss $h_j = \zeta \times v^2/2g = 3.74$ m air column.

Flow resistance $\Delta P = h_f + h_j = 4.25$ m air column = 50 Pa.

Fresh air of 300 m^3/h is needed in the non-filtration state of external circulation, and the total flow resistance is 1175 Pa. If the external circulation needs 300 m^3/h of fresh air in a non-toxic state, the load requirement can be met by increasing the internal circulation air volume.

The external circulation poison filtration requires fresh air of 100m^3/h, and at this time, the wind speed is very low, and the flow resistance of the air duct in the main engine, evaporator core and cabin occupant air duct can be ignored, and the resistance components only include cyclone dust collector and poison filter tank.

(1) The air volume handled by the cyclone is 100 m^3/h, and the resistance is the same as the maximum refrigeration state, which is 116 Pa.

(2) The resistance of the canister shall not be greater than 1300 Pa according to the requirements of relevant specifications.

The external circulation filtration requires fresh air of 100 m^3/h, and the total flow resistance is 1416 Pa.

5 RESULTS ANALYSIS AND RESEARCH

According to the comparison between the above air volume and flow resistance, there is a 300 Pa air supply head under various conditions, and the required booster fan state points are shown in Tab. 2 below.

Table 2 Working state table of booster fan

State point	Use state	Air quantity	Flow resistance	Air supply head	Total head
I	Mixed cycle	500 m^3/h	571 Pa	300 Pa	871 Pa
II	External circulation non-filtering poison	300 m^3/h	1175 Pa	300 Pa	1475 Pa
III	External circulation filtration	100 m^3/h	1416 Pa	300 Pa	1716 Pa

Under the contrast of atmospheric pressure of 300 MPa, the greater the air quantity, the smaller the air pressure resistance. Because the ventilation fan and air conditioning fan are shared, the circulating air quantity needs to consider the air quantity demand of evaporator heat exchange in air conditioning system. The centrifugal booster fan with high pressure head is selected according to the above working conditions, and the flow characteristic curve of the fan is shown in Fig. 9.

From the flow characteristic curve of booster fan, it can be seen that all three working points are contained in the fan capacity range, and there is a certain margin. To create a three-dimensional model of the air duct, the modeling software used is ANSYS Fluent. The simulation of internal and external mixed circulation ventilation flow field is shown in Fig. 10.

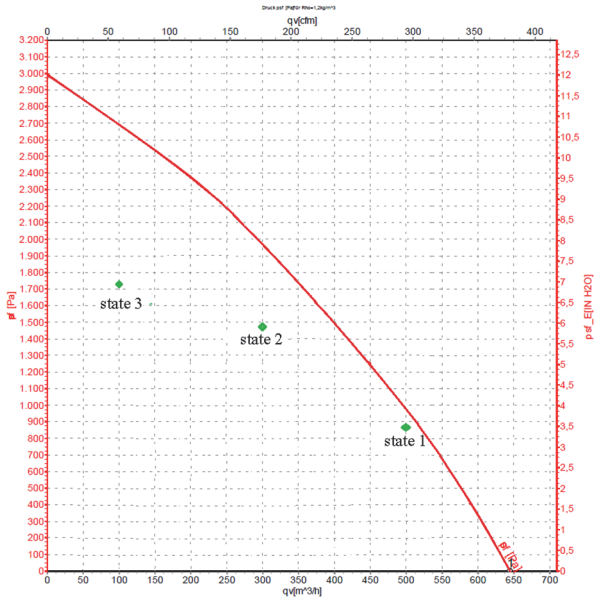

Figure 9 Flow characteristic curve of booster fan

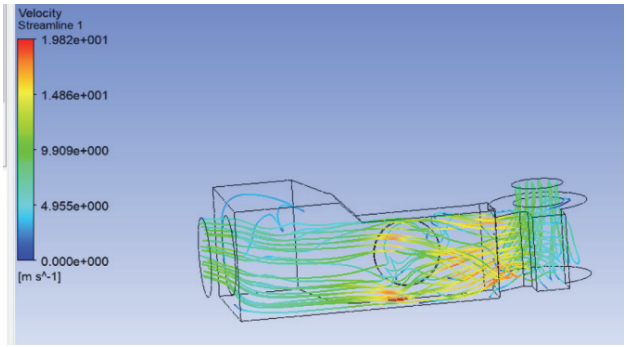

Figure 10 Simulation diagram of internal and external mixed circulation ventilation flow field

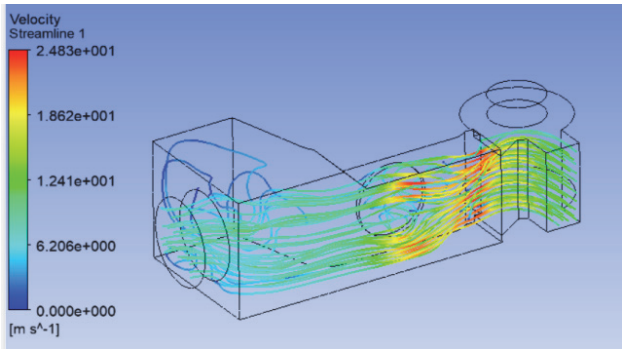

Figure 11 Simulation diagram of internal circulation ventilation flow field

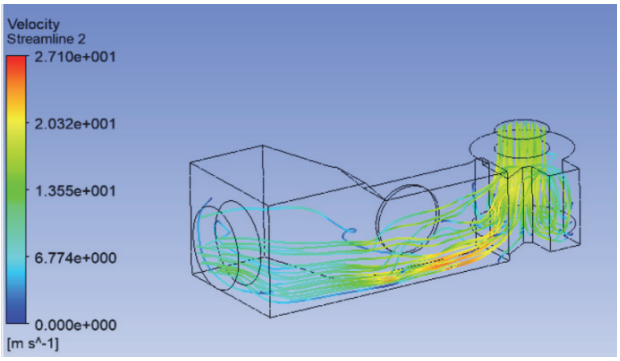

Figure 12 Simulation diagram of external circulation ventilation flow field

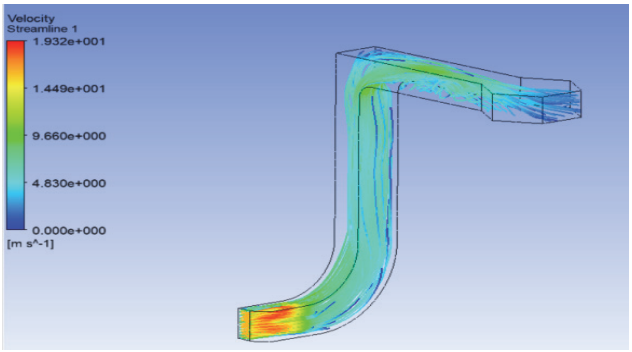

Figure 13 Simulation diagram of flow field in cabin occupant air supply duct

The simulation of internal circulation ventilation flow field is shown in Fig. 11. The simulation of external circulation ventilation flow field is shown in Fig. 12. The simulation of the flow field in the cabin occupant air supply duct is shown in Fig. 13.

The cabin occupant air duct is composed of sealing joint, air supply duct, centralized distribution box, tuyere, oxygen supply pipe and oxygen supply socket. The air supply duct adopts the integrated molding technology of composite materials, and the insulation layer is laid in the middle layer, which not only prevents the insulation layer from being soaked in water, but also makes the inner surface of the pipeline smooth and reduces the flow loss, and the outer surface is beautiful and not easy to scratch. The cross-sectional area of the air supply duct is not less than 15000 mm^2, and five tuyeres are installed in the centralized distribution box. When the air supply flow is 500 m^3/h, the velocity of the tuyeres is 3.3 m/s, and the flow and wind direction of the tuyeres can be adjusted.

6 CONCLUSION

According to the overall technical requirements, the total circulating air supply volume of the cabin is not less than 300 m^3/h. In addition, as the ventilation fan and air-conditioning fan of this system are shared, the circulating air volume needs to consider the air demand for heat exchange of the evaporator of the air-conditioning system. The required circulating air volume can be determined according to the enthalpy value of the evaporator air inlet and outlet state points during refrigeration. According to the refrigeration condition of air conditioner and the design of air conditioning system, the circulating air volume required for heat exchange of air conditioner evaporator is calculated to be about 500 m^3/h, and the circulating air volume of this system is designed according to the rated 500 m^3/h, which can be adjusted from 300 to 500 m^3/h. Through the above calculation and analysis, the ventilation volume and overpressure value under various use conditions are determined. Through CFD simulation and experimental verification, we determine the influence degree of different geometric parameters (such as diameter, length, bending radius, etc.) on friction loss. The results show that reasonable selection of pipe size and shape can significantly reduce the friction loss, thus improving the overall efficiency of the system.

Self-adaptive control of booster fan and exhaust regulating valve. In the modes of external circulation and mixed circulation ventilation, a certain overpressure needs to be established in the cabin, and the fresh air volume needs to meet the needs of passengers. Adaptive control can prevent the fan from overworking when it is not needed, thus reducing energy consumption. By reasonably controlling the operation of the fan, the wear and tear of the equipment can be reduced and its service life can be prolonged. However, the adaptive control of booster fan also has some shortcomings: the adaptive control needs high-precision sensors and complex algorithms, which increases the complexity and cost of the system. Once the adaptive control system fails, it is difficult to maintain and debug, and it needs professional treatment. Using materials with high elasticity (such as rubber, silica gel, etc.) as pipe joints can absorb vibration energy and reduce vibration transmitted to other components. For metal pipes, selecting materials with moderate thickness can reduce the resonance phenomenon caused by thin walls, appropriately shorten the length of the pipeline and reduce the distance of vibration propagation. Reduce airflow noise, and use pipes with smooth inner walls to reduce airflow friction sound. Optimize the cross-sectional shape of the pipeline, such as using a round pipe instead of a square pipe, to reduce the vortex and thus reduce the noise.

Acknowledgements

Key Projects of 2020 Excellent Talents Support Program in Colleges and Universities (gxyqZD2020055); Major projects of natural scientific research in colleges and universities in Anhui Province (2022AH040281); 2022 Provincial Quality Engineering Project-Provincial Teaching and Research Key Project: Research on the Construction of Electrical and Electronics Curriculum Group of "Cloud Classroom+Integration of Theory and Practice" (2022jyxm833); School-level scientific research and innovation team project in 2023: intelligent control and detection technology scientific research and innovation team (2023xjkytd3) 2023 Provincial Quality Engineering Project-Provincial Teaching Innovation Team: Teaching Innovation Team of Electrical Automation Specialty (2023cxtd157); 2024 Key Project of Natural Science Research in Anhui Universities: Application Research on Circuit Component-level Fault Diagnosis of Aviation Airborne Electronic Equipment TCAS System (2024AH050906).

7 REFERENCES

[1] Liu, J., Su, M., & Xu, Q. (2021). Multi-scale feature vector reconstruction for aircraft classification using high range resolution radar signatures. *Journal of Electromagnetic Waves and Applications*, *35*(14), 1843-1862. https://doi.org/10.1080/09205071.2021.1923068

[2] Niveditha, V., Palaniappan, S., Naresh, K., Nayak, C., & Swapna, B. (2021). High speed low area decimation filter for hearing aid application. *International Journal of Speech Technology*, *2*(1), 614-624. https://doi.org/10.1007/s10772-021-09857-5

[3] Chandra Inguva, S. & Seventiline, J. (2021). Implementation of FPGA design of FFT architecture based on CORDIC algorithm. *International Journal of Electronics*, *108*(11), 1914-1939. https://doi.org/10.1080/00207217.2020.1870750

[4] Rajesh, P., Shajin, F. H., Rajani, B., & Sharma, D. (2022). An optimal hybrid control scheme to achieve power quality enhancement in micro grid connected system. *International Journal of Numerical Modelling: Electronic Networks, Devices and Fields*, *5*(2), 656-672.

https://doi.org/10.1002/jnm.3019
[5] Shajin, F. H., Rajesh, P., & Raja, M. R. (2022). An efficient VLSI architecture for fast motion estimation exploiting zero motion prejudgment technique and a new quadrant-based search algorithm in HEVC. *Circuits Systems and Signal Processing*, *41*, 1751-1774. https://doi.org/10.1007/s00034-021-01850-2
[6] Drake, E., Okamoto, N., & Thurlow, E. (2020). The use of CFD to analyze and predict the pressure drop along flat oval duct fittings. *ASHRAE Transactions*, *126*(2), 493-500.
[7] Cao, Z., An, Y., & Wang, Y. (2023). Energy consumption of intermittent ventilation strategies of different air distribution modes for indoor pollutant removal. *Journal of Building Engineering*, *69*, 106242. https://doi.org/10.1016/j.jobe.2023.106242
[8] Feng, Y., Zhu, H., & Feng, X. (2023). Optimization of dual-design operation ventilation system network based on improved genetic algorithm. *Energies*, *16*(24), 7931. https://doi.org/10.3390/en16247931
[9] Alfalouji, Q., Schranz, T., & Falay B. (2023). Co-simulation for buildings and smart energy systems-A taxonomic review. *Simulation Modelling Practice and Theory*, *126*, 102770. https://doi.org/10.1016/j.simpat.2023.102770
[10] Nassif, AB., Shahin, I., & Attili, I. (2019). Speech recognition using deep neural networks: a systematic review. *IEEE Access*, *7*, 19143-19165. https://doi.org/10.1109/ACCESS.2019.2896880
[11] Boretti, A., Castelletto, S., & Al-Zubaidy, S. (2019). Concentrating solar power tower technology: Present status and outlook. *Nonlinear Engineering*, *8*(1), 10-31. https://doi.org/10.1515/nleng-2017-0171
[12] Mokhtar, M. (2018). *Control of solar thermal linear fresnel collector plants in single phase and direct steam generation modes*. Dissertation, KarlsruherInstitut f¨ur Technologie (KIT), KIT Faculty of Mechanical Engineering, Karlsruhe, 6(12), 84-99.
[13] Kan, Yu. S. (2020). An Extension of the Quantile Optimization Problem with a Loss Function Linear in Random Parameters. *Autom. Remote Control*, *81*, 2194-2205. https://doi.org/10.1134/S0005117920120048
[14] Vasileva, S. N. & Kan, Yu. S. (2019). Approximation of Probabilistic Constraints in Stochastic Programming Problems with a Probability Measure Kernel. *Autom. Remote Control*, *80*, 2005-2016. https://doi.org/10.1134/S0005117919110055
[15] Van Ackooij, W., Berge, V., de Oliveira, W., & Sagastizabal, C. (2017). Probabilistic Optimization via Approximate p-Efficient Points and Bundle Methods. *Computers & Operations Research*, *77*, 177-193. https://doi.org/10.1016/j.cor.2016.08.002
[16] Lin, Z. & Zeng, C. (2022). Instability, index theorem, and exponential trichotomy for Linear Hamiltonian PDEs. *Memoirs of the American Mathematical Society*, *275*, 275-294. https://doi.org/10.1090/memo/1347
[17] Pelinovsky, D. (2005). Inertia law for spectral stability of solitary waves in coupled nonlinear Schrödinger equations. *Proceedings of the Royal Society A*, *461*(2055), 783-812. https://doi.org/10.1098/rspa.2004.1345
[18] Galanopoulos, P., Girela, D., & Merchán, N. (2023). Cesàro-type operators associated with Borel measures on the unit disc acting on some Hilbert spaces of analytic functions. *Journal of Mathematical Analysis and Applications*, *526*(2), 127287. https://doi.org/10.1016/j.jmaa.2023.127287
[19] Xie, X. M., Dou, R. W., Yang, Y. P., Xie, J., & Du, X. F. (2022). Harmonic Analysis of Electric Transmission System of New Energy Vehicle, *Strategic Planning for Energy and the Environment*, *40*(3), 279-296. https://doi.org/10.13052/spee1048-4236.4034
[20] Aljemely, A. H., Xuan, J., & Jawad, F. K. J. (2020). A novel unsupervised learning method for intelligent fault diagnosis of rolling element bearings based on deep functional auto-encoder. *Journal of Mechanical Science and Technology*, *34*, 4367-4381. https://doi.org/10.1007/s12206-020-1002-x
[21] Xie, X. M., Wang, Y. Q., Dou, R. W., Hu, K., & Hong, Y. (2022). Research on a Fuzzy Clustering Partition Analysis Method for Circuit Fault Diagnosis. *2021 3rd International Conference on Applied Machine Learning*. https://doi.org/10.1109/ICAML54311.2021.00064
[22] Acu, A. M., Măduţa, A. I., & Raşa, I. (2021). Voronovskaya type results and operators fixing two functions. *Mathematical Modelling and Analysis*, *26*(3), 395-410. https://doi.org/10.3846/mma.2021.13228
[23] Younes, Y. A., Rabhi, A., Noura, H., & Hajjaji, A. E. (2016). Sensor fault diagnosis and fault tolerant control using intelligent-output-estimator applied on quadrotor UAV.*2016 International Conference on Unmanned Aircraft Systems (ICUAS)*, 1117-1123. https://doi.org/10.1109/ICUAS.2016.7502557
[24] Xie, X. M., Gui, S. G., Dou, R. W., & Du, X. F. (2023). Research on Adaptive Fault Diagnosis Control System of Audio Management Component Environment of Airborne Electronic Equipment. *Journal of ICT Standardization, 11*(02), 175-196. https://doi.org/10.13052/jicts2245-800X.1124
[25] Aldaz, J. M., Kounchev, O., & Render, H. (2009). Shape preserving properties of generalized Bernstein operators on extended Chebyshev spaces. *Numerische Mathematik*, *114*(1), 1-25. https://doi.org/10.1007/s00211-009-0248-0
[26] Gavrea, I. & Ivan, M. (2018). Complete asymptotic expansions related to conjecture on a Voronovskaja-type theorem. *Journal of Mathematical Analysis and Applications*, 458(1), 452-463. https://doi.org/10.1016/j.jmaa.2017.09.011
[27] Raj, N., Singh, A. K., & Gupta, A. K. (2016). Low voltage high output impedance bulk-driven quasi-floating gate self-biased high-swing cascode current mirror. *Circuit System and Signal Processing*, 35, 2683-2703. https://doi.org/10.1007/s00034-015-0184-4
[28] Hassen, N. & Gabbouj, H. (2011). Low voltage high performance current mirrors: Application to linear voltage to current converter. *International Journal of Circuit Theory and Application*, *39*, 47-60. https://doi.org/10.1002/cta.618

Contact information:

Xiaomin XIE
(Corresponding author)
Intelligent Manufacturing College,
Anhui Vocational and Technical College,
Hefei 230011, China
E-mail: rogerxxm@sina.com

Xuanfu DU
Intelligent Manufacturing College,
Anhui Vocational and Technical College,
Hefei 230011, China

Shuguo GUI
Intelligent Manufacturing College,
Anhui Vocational and Technical College,
Hefei 230011, China